

Article

# Adaptive Prediction of Enhanced Oil Recovery by N<sub>2</sub> huff-n-puff in Fractured-Cavity Reservoir Using an FNN-FDS Hybrid Model

Qi Wang <sup>1,2</sup>, Hanqiao Jiang <sup>1</sup>, Jianfa Han <sup>3</sup>, Daigang Wang <sup>4,\*</sup> and Junjian Li <sup>1,\*</sup>

<sup>1</sup> College of Petroleum Engineering, China University of Petroleum (Beijing), Beijing 102249, China; wangqi.riped@petrochina.com.cn (Q.W.); jianghq@cup.edu.cn (H.J.)

<sup>2</sup> Research Institute of Petroleum Exploration and Development, PetroChina, Beijing 100083, China

<sup>3</sup> Research Institute of Exploration and Development, PetroChina Tarim Oilfield Company, Korla 841000, China; hanjf-tlm@petrochina.com.cn

<sup>4</sup> Unconventional Petroleum Research Institute, China University of Petroleum (Beijing), Beijing 102249, China

\* Correspondence: dgwang@cup.edu.cn (D.W.); junjian@126.com (J.L.)

**Abstract:** N<sub>2</sub> huff-n-puff has proven to be a promising technique to further improve oil recovery in naturally fractured-cavity carbonate reservoirs. The effect of enhanced oil recovery (EOR) by N<sub>2</sub> huff-n-puff is significantly affected by various dynamic and static factors such as type of reservoir space, reservoir connectivity, water influx, operational parameters, and so on, typically leading to a significant increase in oil production. To reduce the prediction uncertainty of EOR performance by N<sub>2</sub> huff-n-puff, an adaptive hybrid model was proposed based on the fundamental principles of fuzzy neural network (FNN) and fractional differential simulation (FDS); a detailed prediction process of the hybrid model was also illustrated. The accuracy of the proposed FNN-FDS hybrid model was validated using production history of N<sub>2</sub> huff-n-puff in a typical fractured-cavity carbonate reservoir. The proposed model was also employed to predict the EOR performance by N<sub>2</sub> huff-n-puff in a naturally fractured-cavity carbonate reservoir. The methodology can serve as an effective tool to optimize developmental design schemes when using N<sub>2</sub> huff-n-puff to tap more remaining oil in similar types of carbonate reservoirs.

**Keywords:** N<sub>2</sub> huff-n-puff; fractured-cavity reservoir; adaptive performance prediction; fuzzy neural network; fractional differential simulation



**Citation:** Wang, Q.; Jiang, H.; Han, J.; Wang, D.; Li, J. Adaptive Prediction of Enhanced Oil Recovery by N<sub>2</sub> huff-n-puff in Fractured-Cavity Reservoir Using an FNN-FDS Hybrid Model. *Appl. Sci.* **2021**, *11*, 8871. <https://doi.org/10.3390/app11198871>

Academic Editors: Giulio Casini, Ole Petter Wennberg and Antonino Cilona

Received: 8 August 2021

Accepted: 16 September 2021

Published: 24 September 2021

**Publisher's Note:** MDPI stays neutral with regard to jurisdictional claims in published maps and institutional affiliations.



**Copyright:** © 2021 by the authors. Licensee MDPI, Basel, Switzerland. This article is an open access article distributed under the terms and conditions of the Creative Commons Attribution (CC BY) license (<https://creativecommons.org/licenses/by/4.0/>).

## 1. Introduction

The main reservoir spaces of typical fractured-cavity reservoirs consist of karst caves, high-angle fracture networks, and many dissolved pores [1,2]. The reservoir heterogeneity is extremely important, mainly because the distribution is random, the internal structure is very uneven, the spatial configuration pattern of caverns and cracks is complex, and oil–water relationship and flow dynamics are complicated [3,4]. In the early development stage of a fractured-cavity carbonate reservoir, oil production typically depends on natural or bottom water energy. Water injection is one of the more widely used strategies to increase oil production and slow down its decline. However, as the oil–water interface gradually rises, the increase of oil production usually diminishes after water huff-n-puff; a large portion of crude oil remains underground and cannot be produced [5]. Many pilot tests demonstrate that after N<sub>2</sub> gas is injected into a cavity it will move up due to gravity segregation, and gradually occupy the upper space of the cavity, thus displacing crude oil down into the producing wells. N<sub>2</sub> can also be used to replenish reservoir energy, slow down the decline of oil production, and improve oil recovery [6,7]. It is of great importance to make an accurate prediction about N<sub>2</sub> huff-n-puff in order to explore its potential in fractured-cavity carbonate reservoirs.

The artificial neural network-improved fuzzy inference system (ANFIS), firstly developed by Jang (1993) [8], was proven to be an effective tool for exploring inherent behaviors in different areas of study (e.g., water drought, sediment transport, PCP-based NMDA receptor antagonists, elastic constants of rocks, hepatitis C Virus, hydrologic modelling, and hydropower stream flow [9–15]). In recent decades, the ANFIS model has appealed great attentions to improve its predictive ability. By integrating advantages of grey wolf optimization and adaptive neuro-fuzzy inference system, an improved ANFIS is proposed by Dehghani et al. [16], showing better prediction capability. Goodarzi and Freitas [17] studied the feasibility of principal component analysis to design an adaptive neuro-fuzzy inference. By selecting the grid partition (GP), fuzzy c-means (FCM), and subtractive clustering (SC) as three fuzzy inference system structures, Mostafaei [18] developed novel ANFIS models to predict the cetane number of biodiesels. Dastorani et al. [19] applied the artificial neural network (ANN) and ANFIS models to reconstruct missing flow data. Some other self-adaptive methods were also developed in previous oil and gas studies [20,21]. Vardian et al. [22–24] concluded that the ANFIS system can serve as an excellent model with relatively few errors. The ANFIS model has a strong training capability, which is akin to the ANN. Using the back-propagation algorithm, the parameters involved in the ANFIS model were adjusted until an expected error was reached.

The goal of grey prediction is to construct differential equations for prediction, so it can be regarded as one form of differential simulation prediction. There may be multiple controlling factors of the forecasting indicator. Mao et al. [25] presented a novel fractional grey prediction model by substituting the fractional differential equations with their first-order forms. The model is highly accurate and can overcome the class ratio test restrictions of the conventional grey model (GM) (1,1). It demonstrated that the fractional differential simulation (FDS) can greatly improve the prediction ability of differential simulation [26]. Zeng and Li [27] developed a novel GM model originating from a dynamic background-value coefficient. Ma et al. [28] attempted to build a nonlinear grey Bernoulli multivariate prediction model. The GM (1,  $n$ ) model was widely applied in various fields [29–34]. Yang and Xue [35] proposed a generalized fractional-order form of grey prediction model, which provides more freedom by using fractional derivatives. Meng et al. [36] introduced the residual sequence to improve the prediction accuracy of the fractional order grey model. The fractional order grey models were widely used with the improved GM (1,1) model [37,38]. These previous studies show that the prediction ability is strong when the fuzzy neural network (FNN) and fractional differential simulation (FDS) model are integrated. However, the adaptive hybrid model by combining FNN with FDS is still underexplored. In this study, an adaptive hybrid model is developed based on the fundamental theories of FNN and FDS that is then used to predict the EOR performance of  $N_2$  huff-n-puff in a naturally fractured-cavity carbonate reservoir.

## 2. Research Background

The geological heterogeneity of naturally fractured-cavity reservoirs is extremely strong. It was proven that several types of reservoir spaces coexist, mainly including karst cavities, tectonic fractures, and dissolved pores. For typical fractured-cavity carbonate reservoirs that are widely distributed, there is a lack of efficient methods to obtain a high oil recovery during exploitation of these difficult-to-produce reserves due to great lateral and vertical heterogeneity. Figure 1a shows the lateral amplitude distribution retrieved from seismic data of a typical fractured-vuggy carbonate reservoir. The deeper the red color, the greater the amplitude, indicating a larger possibility to represent a cavity. Figure 1b displays the vertical amplitude distribution of a typical fractured-cavity body selected from Figure 1a. Figure 1c reflects the 3-D porosity field of the typical fractured-cavity body as shown in Figure 1b, where the deeper the red color, the higher value the porosity of cell grid in the 3-D geological model of the typical fractured-cavity body.

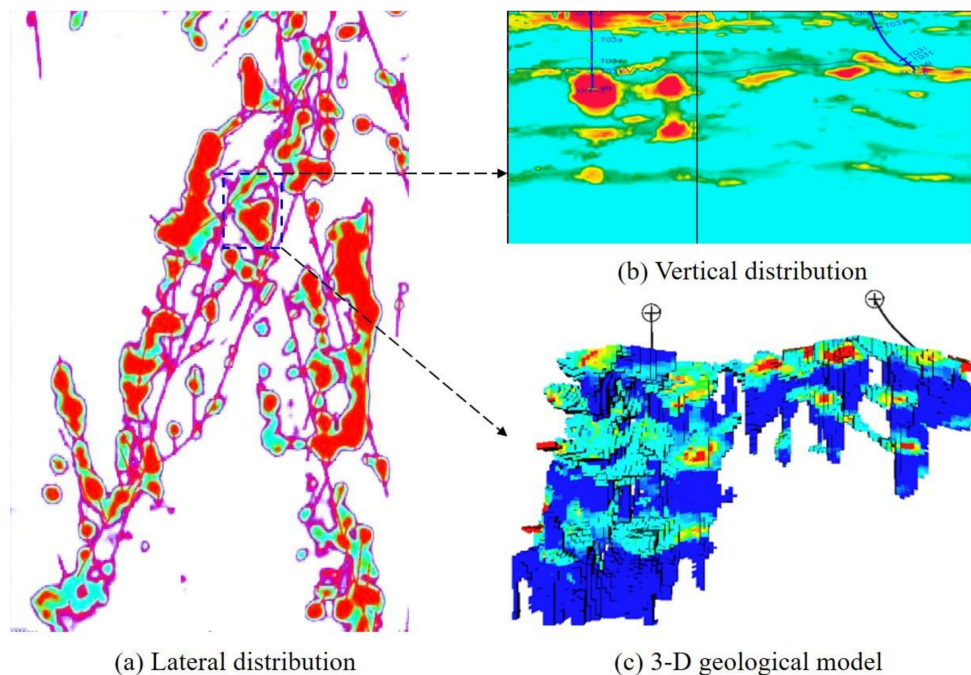


**Figure 1.** Geological characteristics of typical fractured-cavity reservoir. (a) lateral distribution of amplitude; (b) vertical distribution of amplitude; (c) 3-D geological model.

The production performance in the early stage depends heavily on formation energy. To keep oil production stable, water injection is usually selected to supply energy into reservoir space. However, the decline rate of oil production remains stubbornly high due to a poor understanding of reservoir heterogeneity and configuration patterns of multiple fractured-cavity units, leading to a great amount of oil remaining unexploited in the fractured-cavity reservoir.  $N_2$  huff-n-puff is proven to be an efficient technique to further tap the potential of remaining oil. Figure 2 displays the underlying mechanisms of  $N_2$  huff-n-puff in a fractured-cavity carbonate reservoir. It is found that three steps are necessary to carry out one cycle of  $N_2$  huff-n-puff: gas injection, soaking, and production. When  $N_2$  gas is injected into a typical fractured-cavity carbonate reservoir, driven by gravity segregation, it will gradually move to an upper position of the targeted cavity. The secondary gas cap will gradually move down the oil–water interface, and a large amount of crude oil will flow into the bottom hole of producing wells. The supply of formation energy by  $N_2$  huff-n-puff can effectively inhibit the decline of oil production and rise of water cut.

Figure 3 displays the production performance of  $N_2$  huff-n-puff for a producer in a typical fractured-cavity reservoir. It indicates that  $N_2$  huff-n-puff achieves a better oil production rate even if the producer is shut down because of abrupt water-rising. However, the actual effect of increasing oil production by  $N_2$  huff-n-puff differs greatly. It is difficult to achieve an adaptive prediction of EOR performance by  $N_2$  huff-n-puff in a fractured-cavity carbonate reservoir. Many factors can affect the performance of enhanced oil recovery by  $N_2$  huff-n-puff in karst reservoirs (e.g., remaining oil saturation, reservoir thickness, formation pressure, cumulative gas storage rate, daily oil production, natural fracture permeability, injection–production strategy, etc.). By taking all influential factors into account, the actual effect of  $N_2$  huff-n-puff enhanced oil recovery in karst reservoirs can be accurately evaluated, but it is difficult to implement. Selecting certain controlling factors provides an alternative to solve this issue.

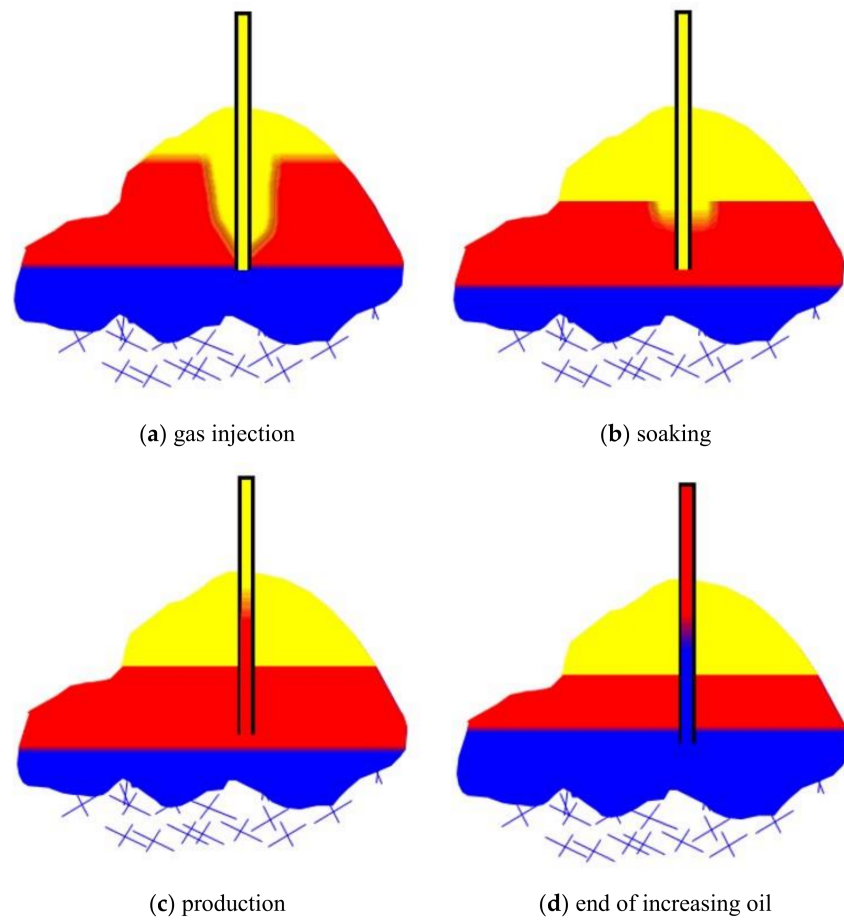


Figure 2. Mechanisms of N<sub>2</sub> huff-n-puff in karst reservoir (red: oil; blue: water; yellow: gas).

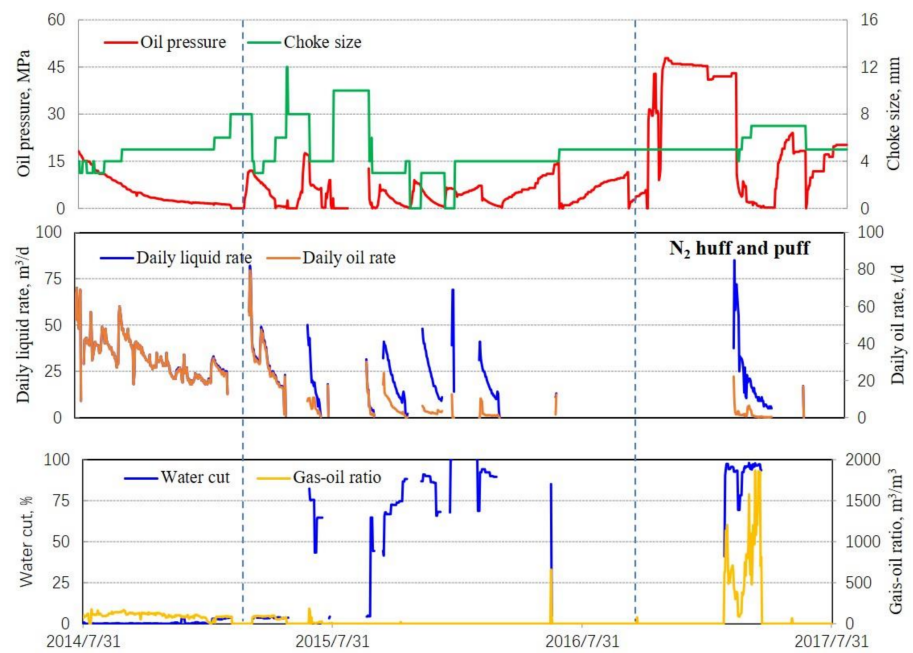


Figure 3. Actual production performance of N<sub>2</sub> huff-n-puff for a typical producer.

### 3. Adaptive FNN-FDS Hybrid Model

Here, the structure flowchart and calculation procedures of the proposed fuzzy neural network (FNN)-fractional differential simulation (FDS) hybrid model will be displayed after the relevant principles are described as follows.

#### 3.1. Adaptive Neuro-Fuzzy Inference System

An artificial neural network is a promising tool due to its self-learning ability, but it lacks a good way to describe the reasoning function. Conversely, the fuzzy system shows good reasoning function with no self-adaptive ability. To resolve this issue, Jang et al (1993) initially developed an adaptive neuro-fuzzy inference system (ANFIS) [8] by integrating the self-learning mechanism of a neural network with the good reasoning ability of the fuzzy system. Moreover, the proposed fuzzy system is converted into an adaptive artificial neural network to carry out the self-learning process. The generalized schematic flowchart of ANFIS that includes five layers is shown in Figure 4. Both the first and the fourth nodes are self-adaptive, but the others are fixed. To make adaptive predictions of EOR performance by N<sub>2</sub> huff-n-puff in a fractured-cavity carbonate reservoir, the ANFIS with only two inputs is utilized.

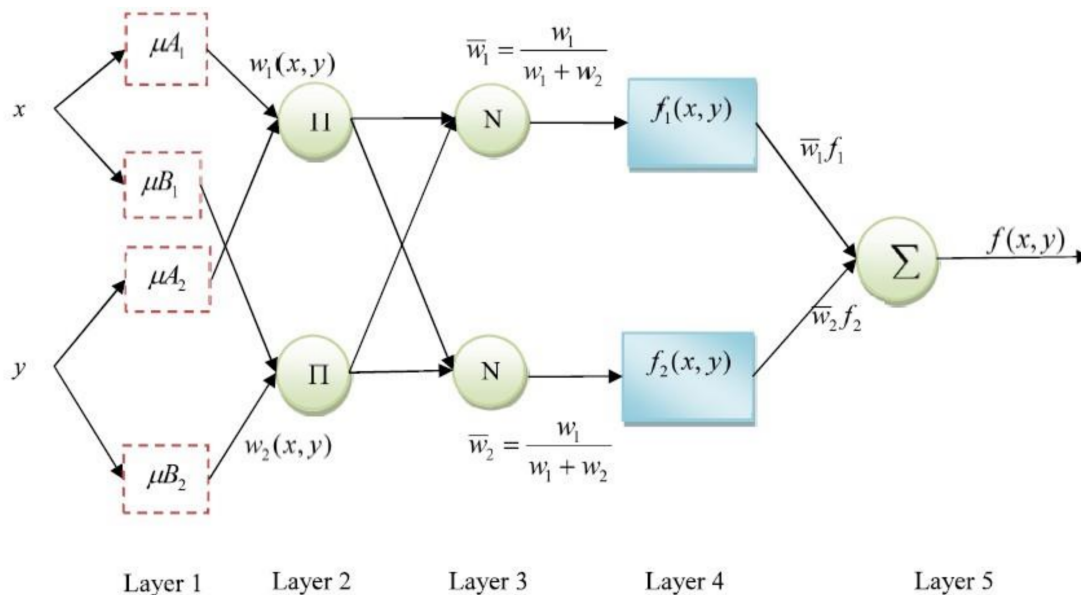


Figure 4. Schematic architecture of the ANFIS model.

The adaptive network is a multilayer feedforward network in which nodes correspond to learning parameters. The significance of each layer will be introduced for an ANFIS model with  $n$  inputs [16,26].

Layer 1 is composed of the input variable membership function, which is selected to fuzzify the input signal. Layer 2 is used to release the regular strength, in which the input signals will be multiplied at the node. Layer 3 is established for normalization, and the fuzzy rule is described as follows:

$$O_i^3 = \bar{w}_i = \frac{\omega_i}{\omega_1 + \omega_2 + \dots + \omega_n}, \quad i = 1, 2, \dots, n \tag{1}$$

Each node in layer 4 is self-adaptive, and the output is expressed as

$$O_i^4 = \bar{w}_i f_i = \bar{w}_i (p_i x + q_i y + r_i), \quad i = 1, 2, \dots, n \tag{2}$$

where  $\bar{w}_i$  is the output of node, and  $\{p_i, q_i, r_i\}$  acts as post-piece parameter set.

Layer 5 denotes a fixed node, indicating the output of signals, which can be defined as a linear combination of the post-piece parameters:

$$O^5 = \sum_{i=1}^n \bar{\omega}_i f = \sum_{i=1}^n ((\bar{\omega}_i x) p_1 + (\bar{\omega}_i y) q_1 + \bar{\omega}_i r_1) \tag{3}$$

where  $O^5$  denotes the prediction data of production by  $N_2$  injection in a fractured-cavity carbonate reservoir.

### 3.2. Fractional Order Differential Simulation Model

Define the sequence  $X_1^{(0)}$  as the decision sequence and the sequence  $X_i^{(0)}$  as the control sequence of the grey system. The  $r$ -order accumulating generation operator of  $X^{(0)}$  is called  $r$ -AGO, ( $r \in R^+$ ).

$$x^{(r)}(k) = \sum_{i=1}^k \frac{\Gamma(r+k-i)}{\Gamma(k-i+1)\Gamma(r)} x^{(0)}(i), k = 1, 2, \dots, m \tag{4}$$

Within the continuous form of  $r$ -AGO sequences, the whiten equation of the grey system can be established as:

$$\frac{dx_1^{(r)}(t)}{dt} + ax_1^{(r)}(t) = \sum_{i=2}^n b_i x_i^{(r)}(t) + u \tag{5}$$

The widely used least squares GM (1,  $n$ ) model is expressed as

$$\hat{a} = (K^T K)^{-1} K^T \Phi \tag{6}$$

The response function is in the following:

$$\hat{x}_1^{(r)}(k+1) = \alpha_1^k x_1^{(0)}(1) + \sum_{i=0}^{k-1} \alpha_1^i \left( \sum_{j=2}^n \alpha_j x_j^{(r)}(k+1-i) \right) + \frac{1 - \alpha_1^k}{1 - \alpha_1} \beta \tag{7}$$

After the series  $\hat{x}_1^{(r)}(k)$  is obtained, the predicted series  $\hat{x}^{(0)}(k+1)$  will be computed using the  $r$ -order inverse accumulating generation operator ( $r$ -IAGO), which takes the form of

$$\hat{x}_1^{(0)}(k+1) = \left( \hat{x}_1^{(r)}(k+1) \right)^{(-r)} \tag{8}$$

where  $\hat{x}_1^{(0)}(k+1)$  represents the prediction result of increasing oil production by  $N_2$  injection in a fractured-cavity carbonate reservoir.

### 3.3. Calculation of Enhanced Oil Recovery Ratio

The ratio of EOR ( $\hat{\eta}$ ) by  $N_2$  huff-n-puff can be calculated by integral of the deviation between the predicted oil production with and without  $N_2$  huff-n-puff when the effect of production decline is considered. This takes the form of

$$\hat{\eta} = \frac{\sum_{i=1}^m \int_{t_1}^{t_2} (\hat{Q}_i - Q_i) dt}{R_0} \tag{9}$$

where  $R_0$  is original oil in place;  $m$  is the well number;  $\hat{Q}_i$  and  $Q_i$  are predicted values of oil production rate with and without  $N_2$  huff-n-puff, respectively; and  $t_1$  and  $t_2$  are the time for start and end of  $N_2$  injection, respectively.

$$Q_i = \bar{Q}_i e^{-at} \tag{10}$$

where  $a$  is the decline rate of oil production, and  $\bar{Q}_i$  is the initial oil production rate.

3.4. Calculation Procedures of FNN-FDS Hybrid Model

According to principles of the adaptive FNN-FDS hybrid model, the structure flowchart is given in Figure 5. The calculation steps are summarized as follows:

Step 1: Convert raw training data into matrix form.

Step 2: Apply training data matrix to FNN model and FDS model, and evaluate the prediction accuracy.

Step 3: Evaluate the prediction accuracy of FNN model and FDS model, which is defined as  $P_1$  and  $P_2$ , respectively. If the maximum value of  $P_1$  and  $P_2$  is lower than  $P_0$  where  $P_0$  is predefined as the converge criterion, detect the singular value of the raw data; otherwise, repeat the calculation of the FNN-FDS hybrid prediction.

Step 4: If  $P_1$  is higher than  $P_2$ , apply prediction data matrix to FNN model, otherwise apply prediction data matrix to FDS model, and calculate the predicted increasing oil production rate of targeted producers by  $N_2$  huff-n-puff;

Step 5: Determine the EOR ratio by  $N_2$  huff-n-puff in fractured-cavity carbonate reservoir and evaluate the oil incremental effect.

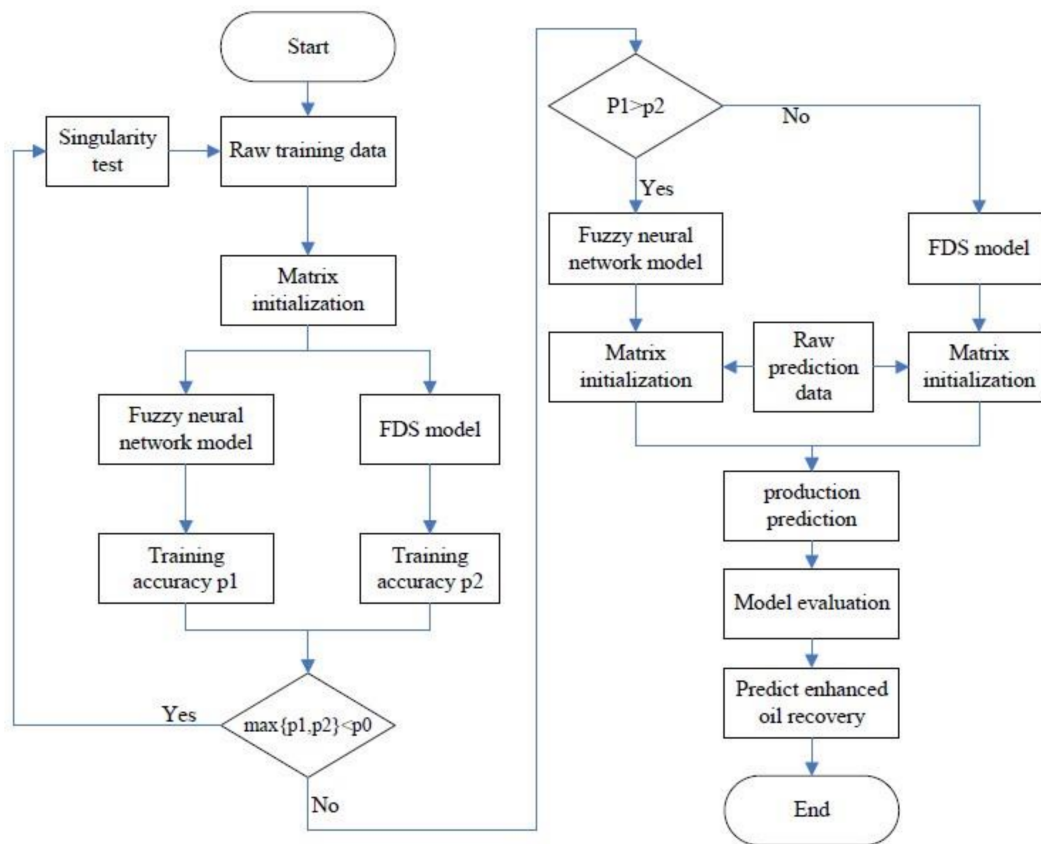


Figure 5. The structure flowchart of the FNN-FDS hybrid model.

## 4. Results and Discussion

In this section, adaptive prediction of enhanced oil recovery by N<sub>2</sub> huff-n-puff in a fractured-cavity carbonate reservoir will be performed using the proposed FNN-FDS hybrid model. The performance appraisal of the predicted results and analysis will also be given.

### 4.1. Raw Data

The factors greatly affecting the degree of increased oil production by N<sub>2</sub> huff-n-puff in a fractured-cavity carbonate reservoir mainly include geological characteristics of reservoir body and various operation parameters of N<sub>2</sub> huff-n-puff. The most important geological characteristics consist of porosity, permeability, and well depth. The main operation parameters include cumulative gas injection, gas storage rate, and cycle of gas injection. There is good evidence that permeability strongly correlates with porosity in a typical fractured-cavity reservoir [39,40], thus permeability is enough to describe the effect of reservoir properties on increasing oil production by N<sub>2</sub> huff-n-puff. Cumulative gas storage can serve as an indicator to the amount of injected gas and gas storage rate. N<sub>2</sub> huff-n-puff is typically used to improve oil recovery of fractured-cavity carbonate reservoirs when water injection becomes invalid, thus cumulative water storage can greatly influence increasing oil production by this method. In this study, the principal component analysis [39,41] is applied to reduce the dimensionality of controlling parameters and to alleviate the dependency of different influential factors. Cumulative gas storage, cumulative water storage, permeability, and total well depth are selected as the main controlling factors of N<sub>2</sub> huff-n-puff in karst reservoirs, which easily originate from production history. Production data for all 22 producing wells were collected in a typical fractured-cavity carbonate reservoir. Table 1 displays the original data of the four controlling factors, in which 17 sets of data were utilized to train the FNN and FDS models and the other five sets of data were selected to validate the accuracy of the proposed FNN-FDS hybrid model for adaptive prediction of EOR performance by N<sub>2</sub> huff-n-puff.

**Table 1.** Raw data of the four controlling factors to N<sub>2</sub> huff-n-puff.

Well No.	Annual Output (m <sup>3</sup> )	Cumulative Gas Storage (10 <sup>4</sup> m <sup>3</sup> )	Cumulative Water Storage (m <sup>3</sup> )	Permeability (mD)	Well Depth (m)
LG01	6231	186	7361	11000	6800
LG02	2281	150	526	5000	6200
LG03	4062	100	2995	8000	6500
LG04	5033	120	2763	9500	6600
LG05	2556	200	1474	5500	6200
LG06	2437	80	740	5300	6200
LG07	6450	600	800	11000	6800
LG08	2086	1000	658	4800	6100
LG09	3929	200	800	7700	6400
LG10	2817	168	46	6000	6200
LG11	6530	600	800	12000	6800
LG12	3427	400	720	7000	6400
LG13	7340	100	4067	13000	7000
LG14	2218	100	636	5000	6200
LG15	2215	600	918	5000	6200
LG16	4725	150	3905	8500	6500
LG17	1986	260	3578	4500	6100
LG18	1045	200	2403	3100	6000
LG19	2935	180	942	6100	6300
LG20	1447	180	1907	3700	6000
LG21	3138	200	605	6500	6300
LG22	4825	100	3968	9000	6600

### 4.2. Model Appraisal

The root-mean-square error [42] (RMSE) and mean absolute percentage error [43] (MAPE) are utilized in this study for performance appraisal of the FNN-FDS hybrid model.

RMSE is one of the most commonly used indicators to validate the accuracy of the predicted data, which takes the form of

$$RMSE = \sqrt{\frac{1}{m} \sum_{i=1}^m (x_{i,p} - x_{i,e})^2} \tag{11}$$

MAPE is used to evaluate the overall accuracy of the predicted values, described as

$$MAPE = \frac{1}{m} \sum_{i=1}^m \left| \frac{x_{i,e} - x_{i,p}}{x_{i,e}} \right| \times 100(\%) \tag{12}$$

where  $x_{i,e}$  is the actual value and  $x_{i,p}$  is the predicted value.

### 4.3. Adaptive Prediction and Discussion

Adaptive prediction of EOR performance by N<sub>2</sub> huff-n-puff in a typical fractured-cavity carbonate reservoir using the FNN-FDS hybrid model is given as follows:

Step 1: Standardize raw data and determine the initial matrix.  $X_x$  is the main controlling factor matrix for enhanced oil recovery by N<sub>2</sub> huff-n-puff in a fractured-cavity reservoir;  $X_y$  is the increased oil production by N<sub>2</sub> huff-n-puff;  $X$  is the initial matrix of raw data;  $X_{xp}$  and  $X_{yp}$  are the initial matrices for training; and  $X_{xv}$  and  $X_{yv}$  are the initial matrices for performance appraisal, respectively.

$$X_x = \begin{bmatrix} X_x^1 \\ X_x^2 \end{bmatrix}, X_y = \begin{bmatrix} X_y^1 \\ X_y^2 \end{bmatrix}, X = \begin{bmatrix} X^1 \\ X^2 \end{bmatrix}$$

where

$$X_x^1 = \begin{bmatrix} 186 & 7361 & 11000 & 6800 \\ 150 & 526 & 5000 & 6200 \\ 100 & 2995 & 8000 & 6500 \\ 120 & 2763 & 9500 & 6600 \\ 200 & 1474 & 5500 & 6200 \\ 80 & 740 & 5300 & 6200 \\ 600 & 800 & 11000 & 6800 \\ 1000 & 658 & 4800 & 6100 \\ 200 & 800 & 7700 & 6400 \\ 168 & 46 & 6000 & 6200 \\ 600 & 800 & 12000 & 6800 \end{bmatrix}, X_x^2 = \begin{bmatrix} 400 & 720 & 7000 & 6400 \\ 100 & 4067 & 13000 & 7000 \\ 100 & 636 & 5000 & 6200 \\ 600 & 918 & 5000 & 6200 \\ 150 & 3968 & 8500 & 6500 \\ 260 & 3578 & 4500 & 6100 \\ 200 & 240 & 3100 & 6000 \\ 180 & 942 & 6100 & 6300 \\ 180 & 1907 & 3700 & 6000 \\ 200 & 605 & 6500 & 6300 \\ 100 & 3968 & 9000 & 6600 \end{bmatrix}$$

$$X_y^1 = [ 6231 \quad 2281 \quad 4062 \quad 5033 \quad 2556 \quad 2437 \quad 6450 \quad 2086 \quad 3929 \quad 2817 \quad 6530 ]^T$$

$$X_y^2 = [ 3427 \quad 7340 \quad 2218 \quad 2215 \quad 4725 \quad 1986 \quad 1045 \quad 2935 \quad 1447 \quad 3138 \quad 4825 ]^T$$

$$X^1 = \begin{bmatrix} 6231 & 186 & 7361 & 11000 & 6800 \\ 2281 & 150 & 526 & 5000 & 6200 \\ 4062 & 100 & 2995 & 8000 & 6500 \\ 5033 & 120 & 2763 & 9500 & 6600 \\ 2556 & 200 & 1474 & 5500 & 6200 \\ 2437 & 80 & 740 & 5300 & 6200 \\ 6450 & 600 & 800 & 11000 & 6800 \\ 2086 & 1000 & 658 & 4800 & 6100 \\ 3929 & 200 & 800 & 7700 & 6400 \\ 2817 & 168 & 46 & 6000 & 6200 \\ 6530 & 600 & 800 & 12000 & 6800 \end{bmatrix}, X^2 = \begin{bmatrix} 3427 & 400 & 720 & 7000 & 6400 \\ 7340 & 100 & 4067 & 13000 & 7000 \\ 2218 & 100 & 636 & 5000 & 6200 \\ 2215 & 600 & 918 & 5000 & 6200 \\ 4825 & 100 & 3968 & 9000 & 6600 \\ 1986 & 260 & 3578 & 4500 & 6100 \\ 1045 & 200 & 2403 & 3100 & 6000 \\ 2935 & 180 & 942 & 6100 & 6300 \\ 1447 & 180 & 1907 & 3700 & 6000 \\ 3138 & 200 & 605 & 6500 & 6300 \\ 4825 & 100 & 3968 & 9000 & 6600 \end{bmatrix}$$

$$X_{xp} = \begin{bmatrix} X_{xp}^1 \\ X_{xp}^2 \end{bmatrix}, X_{yp} = \begin{bmatrix} X_{yp}^1 \\ X_{yp}^2 \end{bmatrix}$$

where

$$X_{xp}^1 = \begin{bmatrix} 186 & 7361 & 11000 & 6800 \\ 150 & 526 & 5000 & 6200 \\ 100 & 2995 & 8000 & 6500 \\ 120 & 2763 & 9500 & 6600 \\ 200 & 1474 & 5500 & 6200 \\ 80 & 740 & 5300 & 6200 \\ 600 & 800 & 11000 & 6800 \\ 1000 & 658 & 4800 & 6100 \\ 200 & 800 & 7700 & 6400 \end{bmatrix}, X_{xp}^2 = \begin{bmatrix} 168 & 46 & 6000 & 6200 \\ 600 & 800 & 12000 & 6800 \\ 400 & 720 & 7000 & 6400 \\ 100 & 4067 & 13000 & 7000 \\ 100 & 636 & 5000 & 6200 \\ 600 & 918 & 5000 & 6200 \\ 150 & 3905 & 8500 & 6500 \\ 260 & 3578 & 4500 & 6100 \end{bmatrix}$$

$$X_y^1 = [ 6231 \quad 2281 \quad 4062 \quad 5033 \quad 2556 \quad 2437 \quad 6450 \quad 2086 \quad 3929 ]^T$$

$$X_y^2 = [ 2817 \quad 6530 \quad 3427 \quad 7340 \quad 2218 \quad 2215 \quad 4725 \quad 1986 ]^T$$

$$X_{xv} = \begin{bmatrix} 260 & 3578 & 4500 & 6100 \\ 200 & 2403 & 3100 & 6000 \\ 180 & 942 & 6100 & 6300 \\ 180 & 1907 & 3700 & 6000 \\ 200 & 605 & 6500 & 6300 \end{bmatrix}, X_{yv} = \begin{bmatrix} 1986 \\ 1045 \\ 2935 \\ 1447 \\ 3138 \end{bmatrix}$$

Step 2: Adaptive production prediction by N<sub>2</sub> huff-n-puff using the structure flowchart (shown in Figure 3) based on the initial matrix X, X<sub>xp</sub>, X<sub>yp</sub>, X<sub>xv</sub>, X<sub>yv</sub>.

Step 3: Obtain the predicted results of increasing oil production by N<sub>2</sub> huff-n-puff with the proposed FNN-FDS hybrid model. Figure 6 compares the predicted and raw data of increasing annual oil production by N<sub>2</sub> huff-n-puff. Figure 7 displays the absolute percentage error of predicted annual oil production.

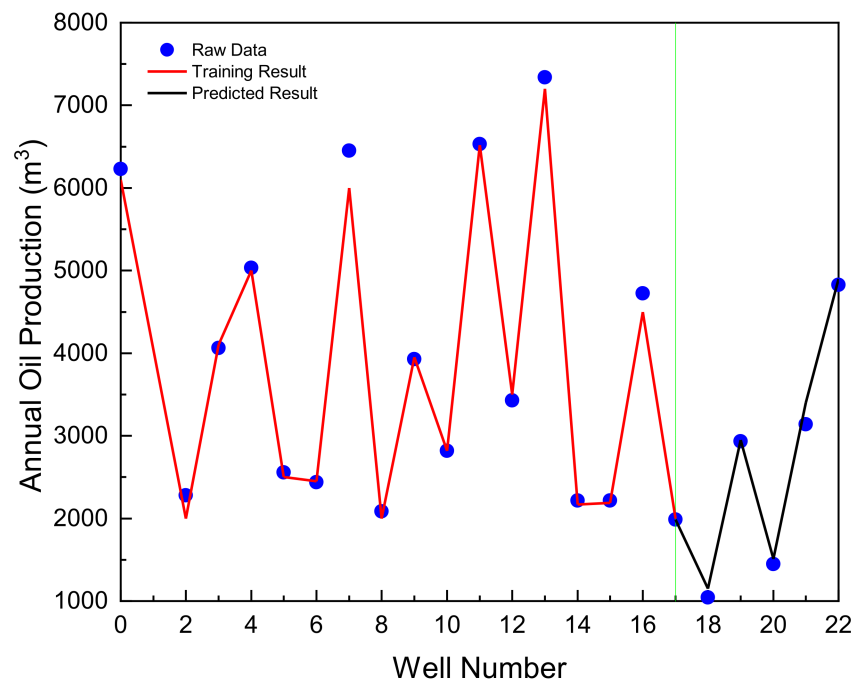


Figure 6. Comparison of predicted and actual annual oil production by N<sub>2</sub> huff-n-puff.

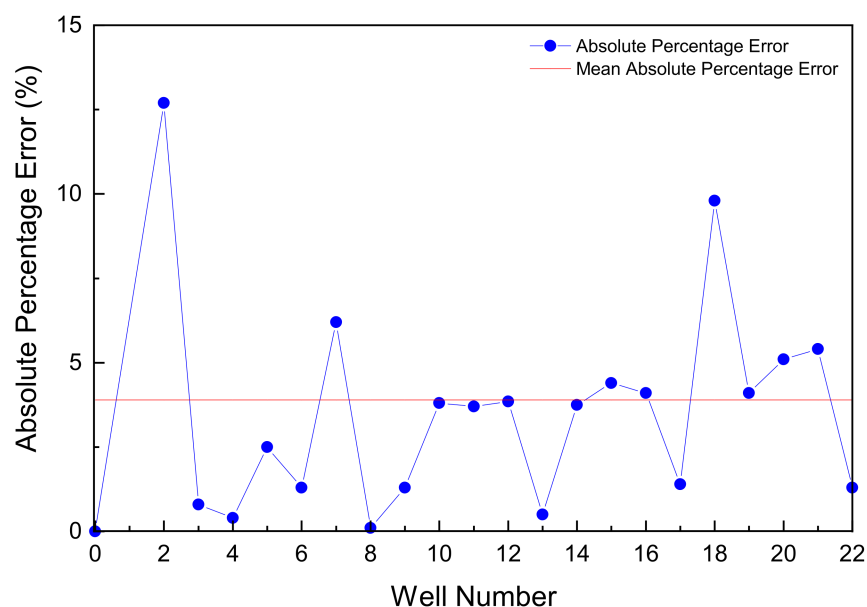


Figure 7. Absolute percentage error of annual oil production prediction.

Step 4: Calculate the predicted value of enhanced oil recovery by  $N_2$  huff-n-puff in a typical fractured-cavity carbonate reservoir. According to the raw data of oilfield production, the annual output decline rate equals 15%. The geological reserve of the oilfield is  $2 \times 10^7 \text{ m}^3$ . The duration time of  $N_2$  huff-n-puff is one year. Table 2 displays the annual oil production of the 22 producers predicted by taking the production decline rate of 15% into consideration. The ratio of enhanced oil recovery ( $\hat{\eta}$ ) by  $N_2$  huff-n-puff is ultimately computed. The predicted value of  $\hat{\eta}$  is 0.1173%.

Table 2. Predicted annual oil production for the 22 producers with decline rate of 15%.

Well No.	Annual Production ( $\text{m}^3$ )	Well No.	Annual Production ( $\text{m}^3$ )
LG01	5121	LG12	2637
LG02	2031	LG13	6824
LG03	3526	LG14	1865
LG04	4542	LG15	1754
LG05	2019	LG16	3951
LG06	2028	LG17	1468
LG07	5965	LG18	896
LG08	1506	LG19	2087
LG09	3017	LG20	1065
LG10	2027	LG21	2614
LG11	5684	LG22	3687

When raw data are used for training, the RMSE and MAPE for the FNN-FDS hybrid model were found to be 144.33 and 2.67, respectively. When raw data are used for prediction, the RMSE and MAPE for the FNN-FDS hybrid model were found to be 107.40 and 4.78, respectively. It can be seen from the results of RMSE and MAPE that the prediction ability of the proposed FNN-FDS hybrid model is satisfactory, showing that the predicted EOR ratio by  $N_2$  huff-n-puff in a fractured-cavity reservoir is credible.

## 5. Conclusions

Fuzzy neural network (FNN)–fractional differential simulation (FDS) hybrid model is proposed to make an adaptive prediction of enhanced oil recovery (EOR) performance by  $N_2$  huff-n-puff in naturally fractured-cavity carbonate reservoirs.

The performance appraisal of N<sub>2</sub> huff-n-puff in a typical carbonate reservoir shows that the prediction ability of the FNN-FDS hybrid model is satisfactory, indicating that the proposed model is efficient for EOR prediction by N<sub>2</sub> huff-n-puff.

The proposed model can guide optimal design of development scheme when using N<sub>2</sub> huff-n-puff to tap more remaining oil in similar carbonate reservoirs.

**Author Contributions:** Conceptualization, Q.W. and J.L.; methodology, Q.W.; software, D.W.; validation, H.J. and J.H.; formal analysis, D.W.; investigation, Q.W.; resources, J.L.; data curation, D.W.; writing—original draft preparation, Q.W.; writing—review and editing, J.L.; visualization, D.W.; supervision, J.L.; project administration, Q.W.; funding acquisition, Q.W. All authors have read and agreed to the published version of the manuscript.

**Funding:** This research is supported by the National Natural Science Foundation of China (Grant No. 52074344) and Science Foundation of China University of Petroleum, Beijing (No.2462020BJRC006).

**Acknowledgments:** The authors sincerely appreciate the Research Institute of Petroleum Exploration and Development (RIPED) and PetroChina for the permission to publish this paper. We also thank all anonymous reviewers for their constructive comments to improve the quality of this paper.

**Conflicts of Interest:** The authors declare no conflict of interest.

## References

1. Zhang, K.; Wang, D. Types of karst-fractured and porous reservoirs in China carbonates and the nature of the Tahe Oilfield in the Tarim Basin. *Acta Geol. Sin.* **2004**, *78*, 866–872.
2. Lv, A.M.; Yao, J.; Wang, W. Characteristics of oil-water relative permeability and influence mechanism in fractured-vuggy me-dium. *Procedia Eng.* **2011**, *18*, 175–183. [[CrossRef](#)]
3. Li, J.; Chen, G.; Zhang, B.; Hong, L.; Han, Q. Structure and fracture-cavity identification of epimetamorphic volcanic-sedimentary rock basement reservoir: A case study from central Hailar Basin, China. *Arab. J. Geosci.* **2019**, *12*, 64. [[CrossRef](#)]
4. Yuan, D.; Hou, J.; Song, Z.; Wang, Y.; Luo, M.; Zheng, Z. Residual oil distribution characteristic of fractured-cavity carbonate reservoir after water flooding and enhanced oil recovery by N<sub>2</sub> flooding of fractured-cavity carbonate reservoir. *J. Pet. Sci. Eng.* **2015**, *129*, 15–22. [[CrossRef](#)]
5. Wang, J.; Liu, H.; Ning, Z.; Zhang, H.; Hong, C. Experiments on water flooding in fractured-vuggy cells in fractured-vuggy reservoirs. *Pet. Explor. Dev.* **2014**, *41*, 74–81. [[CrossRef](#)]
6. Li, Y.B.; Pu, W.F.; Wei, B.; Chen, Y.F.; Bai, B.J. The feasibility of CO<sub>2</sub> and N<sub>2</sub> injection for the tahe fracture-cavity carbonate extra-heavy oil reservoir: An experimental study. *Fuel* **2018**, *226*, 598–606. [[CrossRef](#)]
7. Su, W.; Hou, J.; Zhao, T.; Xi, Y.; Cui, C. Experimental investigation on continuous N<sub>2</sub> injection to improve light oil recovery in multi-wells fractured-cavity unit. *Petroleum* **2017**, *3*, 367–376. [[CrossRef](#)]
8. Jang, J.S.R. ANFIS: Adaptive-network-based fuzzy inference system. *IEEE Trans. Syst. Man Cybern.* **1993**, *23*, 665–685. [[CrossRef](#)]
9. Shabri, A.A. Hybrid wavelet analysis and adaptive neuro-fuzzy inference system for drought forecasting. *Appl. Math. Sci.* **2014**, *8*, 6909–6918. [[CrossRef](#)]
10. Azamathulla, H.M.; Ghani, A.A.; Fei, S.Y. ANFIS-based approach for predicting sediment transport in clean sewer. *Appl. Soft Comput.* **2012**, *12*, 1227–1230. [[CrossRef](#)]
11. Buyukbingol, E.; Sisman, A.; Akyildiz, M.; Alparslan, F.N.; Adejare, A. Adaptive neuro-fuzzy inference system (ANFIS): A new approach to predictive modeling in QSAR applications: A study of neuro-fuzzy modeling of PCP-based NMDA receptor antagonists. *Bioorganic Med. Chem.* **2007**, *15*, 4265–4282. [[CrossRef](#)]
12. Singh, R.; Kainthola, A.; Singh, T. Estimation of elastic constant of rocks using an ANFIS approach. *Appl. Soft Comput.* **2012**, *12*, 40–45. [[CrossRef](#)]
13. Elaziz, M.A.; Moemen, Y.S.; Hassanien, A.E.; Xiong, S.W. Quantitative Structure-Activity Relationship Model for HCVNS5B inhibitors based on an Antlion Optimizer-Adaptive Neuro-Fuzzy Inference System. *Sci. Rep.* **2018**, *8*, 1506. [[CrossRef](#)]
14. Mosavi, A.; Ozturk, P.; Chau, K.-W. Flood Prediction Using Machine Learning Models: Literature Review. *Water* **2018**, *10*, 1536. [[CrossRef](#)]
15. Hammid, A.T.; Sulaiman, M.H.B.; Abdalla, A.N. Prediction of small hydropower plant power production in Himreen Lake dam (HLD) using artificial neural network. *Alex. Eng. J.* **2018**, *57*, 211–221. [[CrossRef](#)]
16. Dehghani, M.; Riahi-Madvar, H.; Hooshyaripor, F.; Mosavi, A.; Shamshirband, S.; Zavadskas, E.K.; Chau, K.-W. Prediction of Hydropower Generation Using Grey Wolf Optimization Adaptive Neuro-Fuzzy Inference System. *Energies* **2019**, *12*, 289. [[CrossRef](#)]
17. Goodarzi, M.; Freitas, M. MIA-QSAR coupled to principal component analysis-adaptive neuro-fuzzy inference. *Eur. J. Med. Chem.* **2010**, *45*, 1352–1358. [[CrossRef](#)] [[PubMed](#)]
18. Mostafaei, M. ANFIS models for prediction of biodiesel fuels cetane number using desirability function. *Fuel* **2018**, *216*, 665–672. [[CrossRef](#)]

19. Dastorani, M.T.; Moghadamnia, A.; Piri, J.; Rico-Ramirez, M. Application of ANN and ANFIS models for reconstructing missing flow data. *Environ. Monit. Assess.* **2010**, *166*, 421–434. [[CrossRef](#)] [[PubMed](#)]
20. Janiga, D.; Czarnota, R.; Stopa, J.; Wojnarowski, P. Self-adapt reservoir clusterization method to enhance robustness of well placement optimization. *J. Pet. Sci. Eng.* **2018**, *173*, 37–52. [[CrossRef](#)]
21. Sayyafzadeh, M. Reducing the computation time of well placement optimization problems using self-adaptive metamodeling. *J. Pet. Sci. Eng.* **2017**, *151*, 143–158. [[CrossRef](#)]
22. Vardian, M.; Nasriani, H.R.; Faghihi, R.; Jowkar, S. Porosity and permeability prediction from well logs using an adaptive neuro-fuzzy inference system in a naturally fractured gas-condensate reservoir. *Energy Sources Part A Recover. Util. Environ. Eff.* **2016**, *38*, 435–441. [[CrossRef](#)]
23. Khoshneviszadeh, M.; Sakhteman, A. Exploring quantitative structure–activity relationship (QSAR) models for some biologically active catechol structures using PC-LS-SVM and PC-ANFIS. *Appl. Biol. Chem.* **2016**, *59*, 433–441. [[CrossRef](#)]
24. Wang, X.; Du, P.; Shen, J. Smoothing splines with varying smoothing parameter. *Biometrika* **2013**, *100*, 955–970. [[CrossRef](#)]
25. Mao, S.; Gao, M.; Xiao, X.; Zhu, M. A novel fractional grey system model and its application. *Appl. Math. Model.* **2016**, *40*, 5063–5076. [[CrossRef](#)]
26. Ma, X.; Liu, Z.B. The GMC (1, n) model with optimized parameters and its applications. *J. Grey Syst.* **2017**, *29*, 121–137.
27. Zeng, B.; Li, C. Improved multi-variable grey forecasting model with a dynamic background-value coefficient and its application. *Comput. Ind. Eng.* **2018**, *118*, 278–290. [[CrossRef](#)]
28. Ma, X.; Liu, Z.; Wang, Y. Application of a novel nonlinear multivariate grey Bernoulli model to predict the tourist income of China. *J. Comput. Appl. Math.* **2018**, *347*, 84–94. [[CrossRef](#)]
29. Deng, C.Y.; Zhang, S.T.; Deng, J.L. Numerical mapping in DNA sequences and analysis of the genetic information by GM (1, n). *J. Grey Syst.* **2012**, *24*, 217–224.
30. Li, Q.F.; Dang, Y.G.; Wang, Z.X. Analysis of the regional coordination development systems based on GRA and GM (1, n). *J. Grey Syst.* **2012**, *24*, 95–100.
31. Hsu, K.T. Using GM (1, n) to assess the effects of economic variables on bank failure. *J. Grey Syst.* **2011**, *23*, 355–368.
32. Tong, J.; Fu, J.H.; Wang, Q.; Wang, Z.Y. A grey estimation method for the seismic intensity. *J. Grey Syst.* **2011**, *23*, 251–256.
33. Tien, T.L. A research on the grey prediction model GM (1, n). *Appl. Math. Comput.* **2012**, *218*, 4903–4916. [[CrossRef](#)]
34. Ma, X.; Liu, Z.B. Research on the novel recursive discrete multivariate grey prediction model and its applications. *Appl. Math. Model.* **2016**, *40*, 4876–4890. [[CrossRef](#)]
35. Yang, Y.; Xue, D. Continuous fractional-order grey model and electricity prediction research based on the observation error feedback. *Energy* **2016**, *115*, 722–733. [[CrossRef](#)]
36. Meng, W.; Yang, D.; Huang, H. Prediction of China's Sulfur Dioxide Emissions by Discrete Grey Model with Fractional Order Generation Operators. *Complexity* **2018**, *2018*, 8610679. [[CrossRef](#)]
37. Yang, Y.; Xue, D. An actual load forecasting methodology by interval grey modeling based on the fractional calculus. *ISA Trans.* **2018**, *82*, 200–209. [[CrossRef](#)]
38. Chen, L.; Liu, Z.B.; Ma, N.N. Time-Delayed Polynomial Grey System Model with the Fractional Order Accumulation. *Mathematical Problems in Engineering*. 2018, 1–7. *Math. Probl. Eng.* **2018**, 1–7.
39. Wang, D.; Li, Y.; Hu, Y. Integrated dynamic evaluation of depletion-drive performance in naturally fractured-vuggy carbonate reservoirs using DPSO-FCM clustering. *Fuel* **2016**, *181*, 996–1010. [[CrossRef](#)]
40. Wang, D.; Li, Y.; Chen, B. Ensemble-based optimization of interwell connectivity in heterogeneous waterflooding reservoirs. *J. Nat. Gas Sci. Eng.* **2017**, *38*, 245–256. [[CrossRef](#)]
41. Shafiei, A.; Dusseault, M.B.; Zendehboudi, S. A new screening tool for evaluation of steamflooding performance in Naturally Fractured Carbonate Reservoirs. *Fuel* **2013**, *108*, 502–514. [[CrossRef](#)]
42. Hyndman, R.; Koehler, A.B. Another look at measures of forecast accuracy. *Int. J. Forecast.* **2006**, *22*, 679–688. [[CrossRef](#)]
43. de Myttenaere, A.; Golden, B.; Le Grand, B.; Rossi, F. Mean Absolute Percentage Error for regression models. *Neurocomputing* **2016**, *192*, 38–48. [[CrossRef](#)]